January 5, 2016

Model independent extraction of the axial mass parameter in anti-neutrino-nucleus scattering

Anthony J. Tropiano

Michigan State University

Advisor

Dr. Gil Paz

Wayne State University

Abstract

Quasielastic (anti) neutrino-nucleon scattering is a process used by many experiments in studying neutrino oscillations. The extracted axial mass parameter has shown discrepancy amongst different experiments assuming a dipole model for the axial form factor. We conduct a model independent extraction of the axial mass parameter from MiniBooNE data for anti-neutrino scattering on ^{12}C and mineral oil. A model designed to include the hydrogen contribution in mineral oil scattering is presented. We find the value for m_A to be consistent from carbon to mineral oil data and both in good agreement with the neutrino scattering result; $m_{A,\text{ carbon}} = 0.85^{+0.13}_{-0.06}$ GeV, $m_{A,\text{ min. oil}} = 0.84^{+0.15}_{-0.04}$ GeV and $m_{A,\text{ neutrino result}} = 0.85^{+0.22}_{-0.07}$. These values differ greatly from the dipole extracted axial mass; $m_A{}^{\text{dipole}}{}_{\text{carbon}} = 1.31^{+0.04}_{-0.05}$ GeV and $m_A{}^{\text{dipole}}{}_{\text{min. oil}} = 1.27^{+0.03}_{-0.04}$ GeV.

1 Introduction

Experiments of the past few decades have revealed evidence of a quantum mechanical phenomenon known as neutrino oscillations. In this process, a neutrino with specific flavor (electron, muon, or tau) can later be measured to have a different flavor. The probability of such an oscillation varies periodically as the neutrino propagates through space. The observation of neutrino oscillations implies that neutrinos have non-zero mass contrary to the Standard Model of particle physics. The 2015 Nobel Prize in physics was awarded to Takaaki Kajita and Arthur B. McDonald for their discovery of neutrino oscillations. Understanding this phenomenon could reveal physics beyond the Standard Model.

Neutrino oscillation experiments need the charged current quasielastic (anti) neutrino-nucleon scattering cross section as an input. In CCQE scattering, a(n) (anti) neutrino scatters from a nucleon to produce a lepton of the same flavor as the neutrino. We consider data from MiniBooNE [1], an experiment at Fermilab that performed the following scattering processes,

$$\nu_\mu + n \rightarrow \mu^- + p, \tag{1}$$

$$\bar{\nu}_\mu + p \rightarrow \mu^+ + n. \tag{2}$$

The MiniBooNE collaboration has provided measurements of (anti)-muon-neutrino CCQE double-differential cross section in terms of muon angle and energy. This paper discusses anti-neutrino-proton scattering (2) in particular. The MiniBooNE experiment directs a proton beam from the Fermilab Booster at a beryllium target. Inelastic scattering emits several particles which are redirected by a magnetic focusing horn and sent into an absorber. At this point, the neutrinos are filtered through to the detector. The detector is a spherically shaped tank filled with 800 tons of mineral oil and lined with 1,280 photomultiplier tubes.

The axial mass parameter, m_A, is extracted from fitting experimental data, and then the resultant value is used as a means of comparison. This parameter is commonly found in the dipole ansatz of the form factor of the nucleon,

$$F_A{}^{\text{dipole}}(q^2) = \frac{F_A(0)}{[1-\frac{q^2}{(m_A{}^{\text{dipole}})^2}]^2}. \tag{3}$$

Since $F_A(0)$ is known from neutron decay, equation (3) provides a simple method for extracting $m_A{}^{\text{dipole}}$. Recent evidence shows differing results for the axial mass parameter amongst these neutrino oscillation experiments. World averages recorded by Bernard et al. [2] and the NOMAD collaboration [3] report values for $m_A{}^{\text{dipole}}$ close to 1.0 GeV. MiniBooNE [4], on the other hand, reports $m_A{}^{\text{dipole}} = 1.35 \pm 0.17$ GeV. Furthermore, K2K SciFi [5], K2K SciBar [6], and MINOS [7] collaborations give a significantly higher value than the world average. The axial mass parameter is a fundamental property of the nucleon regardless of the beam energy or nuclear target. Hence, it is critical to obtain consistency amongst experiments.

The parameterizations of the dipole form factor are overly constrained since (3) depends on one parameter. Additionally, the axial mass parameter in (3) is not well-defined since the true form factor of the proton does not necessarily have a pure dipole behavior. Forcing precise measurements to fit this form factor will lead to discrepancy in $m_A{}^{\text{dipole}}$ as a result of different

ranges of q^2. We define the axial mass parameter in terms of the form factor slope at $q^2 = 0$: $m_A \equiv \sqrt{\frac{2F_A(0)}{F'_A(0)}}$. In contrast to the dipole model, we apply model-independent z expansion to the axial-vector form factor. The use of z expansion introduces more parameters in the axial-vector form factor allowing more freedom in fits. Further details of this method can be found in [8], [9] and [10]. The anti-neutrino-nucleus scattering has two levels: the interaction of the anti-neutrino and the nucleus, or the anti-neutrino and a nucleon. To extract m_A, one must sufficiently describe both the nuclear-level interaction and the nucleon-level interaction. In the past, theoretical studies have addressed nuclear modeling, but all used the dipole form factor mentioned above. The nucleon-level interaction must be resolved before nuclear physics effects are considered. Consequently, we adopt the widely-used Relativistic Fermi Gas (RFG) model of Smith and Moniz [11] in this analysis. We vary the nucleon-level interaction by applying the dipole model and the z expanded axial form factor. This will isolate the contribution of the axial-vector form factor.

The paper is structured as follows. In section 2, we utilize methods of analyticity in our model independent description of the form factor, F_A. In Section 3, we describe the chi-squared minimization fit used to extract m_A. In Section 4, results are analyzed. Lastly, in section 5, a final comparison of the results is made and future work in this area is discussed.

2 Z Expansion

2.1 Axial-Vector Form Factor

The nucleon matrix element of the Standard Model weak charged current is

$$\langle p(p')|J_W{}^{+\mu}|n(p)\rangle \propto \bar{u}^{(p)}(p')\left\{\gamma^\mu F_1(q^2)+\frac{i}{2m_N}\sigma^{\mu\nu}q_\nu F_2(q^2)+\gamma^\mu\gamma_5 F_A(q^2)+\frac{1}{m_N}q^\mu\gamma_5 F_P(q^2)\right\}u^{(n)}(p), \tag{4}$$

where $q^\mu = p'^\mu - p^\mu$, and we have enforced time-reversal invariance and neglected isospin-violating effects. The vector form factors, F_1 and F_2, can be related by isospin symmetry to the electromagnetic form factors measured in electron-proton scattering. Additionally, the impact of F_P is suppressed by powers of the small lepton-nucleon mass ratio. This leaves F_A as the only non-constrained form factor.

In the MiniBooNE energy range, the axial form factor is the dominant contribution to the cross section. The most common way of extracting m_A is to replace the axial-vector form factor with the dipole ansatz, F_A^{dipole}. However, this procedure suffers from the functional dependence of $F_A^{\text{dipole}}(q^2)$ being poorly constrained at relevant neutrino energies. Alternatively, we use applications of analyticity on the axial-vector form factor to extract m_A.

2.2 Analyticity

We write the form factor using the dispersion relation from [8] and [9],

$$F_A(t) = \frac{1}{\pi}\int_{t_{cut}}^{\infty}\frac{\text{Im } F_A(t'+i0)}{t'-t}\,dt', \tag{5}$$

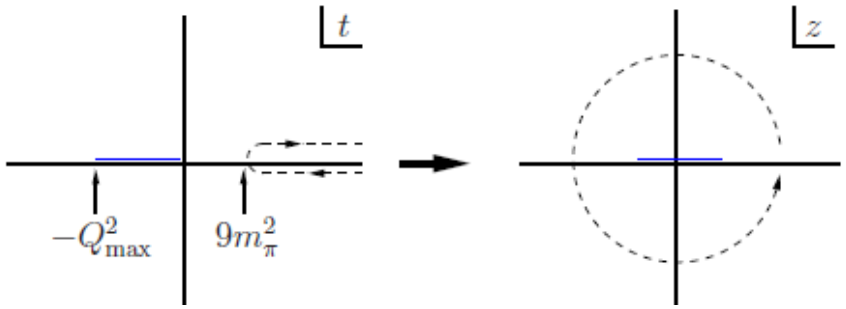

Figure 1: Conformal mapping of the cut plane to the unit circle.

where $t \equiv q^2$ and the integral starts at the three-pion cut, $t_{cut} = 9m^2_\pi$. $F_A(t)$ is complex differentiable in the region outside the cut $[t_{cut}, \infty]$ lying on the real axis. This implies that $F_A(t)$ is analytic everywhere outside $[t_{cut}, \infty]$.

We map the domain of analyticity onto the unit circle via

$$z(t, t_{cut}, t_0) = \frac{\sqrt{t_{cut}-t}-\sqrt{t_{cut}-t_0}}{\sqrt{t_{cut}-t}+\sqrt{t_{cut}-t_0}}, \tag{6}$$

where t_0 is a free parameter representing the point mapping onto $z = 0$ (as seen in figure 1). Any analytic function in this domain will converge to its own power series. Therefore, the form factor can be written as a power series in the new variable,

$$F_A(q^2) = \sum_{k=0}^{\infty} a_k z(q^2)^k. \tag{7}$$

The coefficients multiplying z^k are bounded in size which guarantees convergence of the series. The coefficients are given by

$$a_0 = \frac{1}{\pi}\int_0^\pi \mathrm{Re}\, F_A[t(\theta) + i0]\, d\theta = F_A(t_0), \tag{8}$$

$$a_{k\geq 1} = -\frac{2}{\pi}\int_0^\pi \mathrm{Im}\, F_A[t(\theta) + i0]\sin(k\theta)\, d\theta = \frac{2}{\pi}\int_{t_{cut}}^{\infty} \frac{1}{t-t_0}\sqrt{\frac{t_{cut}-t_0}{t-t_{cut}}}\, \mathrm{Im}\, F_A(t)\sin[k\theta(t)]\, dt, \tag{9}$$

where

$$t = t_0 + \frac{2(t_{cut}-t_0)}{1-\cos\theta} \equiv t(\theta). \tag{10}$$

A major advantage of this method is that the expansion coefficients can be bounded using knowledge of Im F_A. With the z expansion, only a finite number of parameters are necessary to describe the form factor with a given precision. Throughout the paper, bounds of 5 and 10 are used on the expansion coefficients, that is, $|a_k| \leq 5$ and $|a_k| \leq 10$. A more detailed explanation of z expansion and the choice of bounds can be found in [8].

3 Extraction of the axial mass parameter

The mineral oil in the MiniBooNE detector is composed of C_nH_{2n+2}, $n \sim 20$. We must consider two types of protons for the scattering; the proton bound in carbon and the free proton in

hydrogen. MiniBooNE has released a mineral oil data set which includes scattering from all protons. Additionally, MiniBooNE has released a carbon data set excluding scattering from free protons. The flux-integrated double-differential cross section per nucleon is given by

$$\left(\frac{d^2\sigma}{dT_\mu d\cos\theta_\mu}\right)_i = \frac{\sum_j U_{ij}(d_j - b_j)}{(\Delta T_\mu)_i(\Delta\cos\theta_\mu)_i \epsilon_i \Phi N}, \tag{11}$$

where d_j refers to data, b_j the background, U_{ij} is an unfolding matrix connecting the reconstructed variable index j to the true index i, ϵ_i is the detection efficiency, ΔT_μ and $\Delta\cos\theta_\mu$ the respective bin widths, Φ the integrated $\bar{\nu}_\mu$ exposure, and N the number of proton targets in the volume studied. In obtaining the carbon data set, $\bar{\nu}_\mu$ hydrogen events are included in the background term b_j in (11) whereas the other terms in the calculation based on signal definition are now based only on $\bar{\nu}_\mu$ CCQE events involving protons bound in carbon [1, 12].

We compare axial mass results as extracted from both data sets using the dipole form factor and the z expanded form factor. Let m_A^{dipole} refer to the axial mass as extracted from using the dipole model (3) whereas m_A refers to the axial mass as extracted as a slope of F_A. When using the dipole model, $m_A^{dipole} \equiv m_A$. All procedures reported in this paper apply the Relativistic Fermi Gas model [11].

We calculate the theoretical prediction of the cross section with

$$\frac{d\sigma_{nuclear}}{dE_\mu d\cos\theta_\mu} = \frac{G_F{}^2 \, |\vec{P}_\mu|}{16\pi^2 m_T}\{2(E_\mu - |\vec{P}_\mu|\cos\theta_\mu)W_1 + (E_\mu + |\vec{P}_\mu|\cos\theta_\mu)W_2 - \frac{1}{m_T}[(E_\mu - |\vec{P}_\mu|\cos\theta_\mu)(E_\nu + E_\mu) - m_\mu{}^2]W_3 + \frac{m_\mu{}^2}{m_T{}^2}(E_\mu - |\vec{P}_\mu|\cos\theta_\mu)W_4 - \frac{m_\mu{}^2}{m_T}W_5\}, \tag{12}$$

where E_μ is the muon energy, $\vec{P}_\mu$ is the muon momentum, $\cos\theta_\mu$ is the muon direction, and the W_i are given in [8]. Next, we integrate over the normalized $\bar{\nu}_\mu$ flux from Table XI of [1] to give the flux-averaged cross section. Assuming carbon nucleus scattering, the result is divided by 6 to obtain the per-proton event rate. The corresponding experimental values of the double-differential cross section are found in Table XIII (mineral oil) and Table XIX (carbon) from [1]. We apply χ^2 minimization to find values for m_A. The χ^2 function is given by

$$\chi^2 = \Sigma\,(\sigma_i{}^{expt} - \sigma_i{}^{theory})E_{ij}{}^{-1}(\sigma_j{}^{expt} - \sigma_j{}^{theory}), \tag{13}$$

where

$$E_{ij} = (\delta\sigma_i)^2\delta_{ij} + (\delta N)^2\sigma_i\sigma_j \tag{14}$$

is the error matrix, σ_i denotes the partial cross section, $\delta\sigma_i$ denotes the shape uncertainty of the partial cross section (Tables XIV and XX from [1]), and δN is the normalization error. The uncertainty in m_A is given by the $\Delta\chi^2 = 1$ interval. The nucleon form factors are given in [13] and the relevant parameter values in [8]. We use $\epsilon_b = 0.025$ GeV as was done in [8]. For the z expansion of F_A, we let $k_{max} = 7$ in the sum (7). This truncation does not differ significantly from $k_{max} = 8$, 9, and so on.

We define a reconstructed $Q^2 = -q^2$ where

$$Q^2{}_{rec} = 2E_\nu{}^{rec}E_\mu - 2E_\nu{}^{rec}\sqrt{E^2{}_\mu - m^2{}_\mu}\cos\theta_\mu - m^2{}_\mu, \tag{15}$$

and $E_\nu{}^{rec}$ approximates the anti-neutrino energy in the nucleon rest frame,

$$E_\nu{}^{rec} = \frac{m_N E_\mu - \frac{1}{2}m^2{}_\mu}{m_N - E_\mu + \sqrt{E^2{}_\mu - m^2{}_\mu}\cos\theta_\mu}. \tag{16}$$

4 Results

The mineral oil is composed of carbon and hydrogen atoms, (C_nH_{2n+2}, n~20). For anti-neutrinos, we must consider scattering from both bound protons in carbon and free protons in hydrogen (2). In section 4.1, we extract the axial mass from the carbon data. In section 4.2, we extract the axial mass from mineral oil data in two manners. First, we assume the free protons have no contribution in the theoretical prediction of the chi-squared function (13). Second, we include the free proton's contribution using a statistical model. A comparison of these three circumstances is made in section 5.

4.1 Carbon data

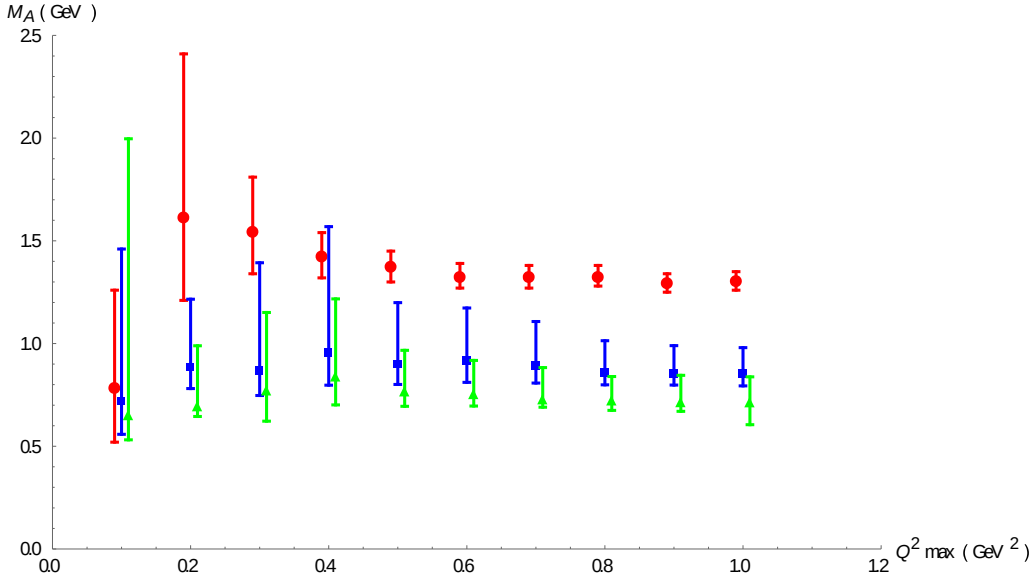

Figure 2: Extracted values of m_A versus Q^2_{max} from carbon data. Dipole model results for $m_A{}^{dipole}$ are shown by red circles; z expansion results with $|a_k| \leq 5$ are shown by blue squares, and z expansion results with $|a_k| \leq 10$ are shown by green triangles.

Results for m_A are presented in figure 2 as extracted using both the dipole form factor and z expanded form factor. The coefficients, a_k, are bounded in size such that $|a_k| \leq 5$ and $|a_k| \leq 10$. The values of m_A are varied with $Q^2{}_{max}$ where $Q^2{}_{rec} \leq Q^2{}_{max}$. The axial mass is directly compared at $Q^2{}_{max} = 1.0$ GeV^2 below

$$m_A{}^{dipole} = 1.31^{+0.04}_{-0.05}\ \text{GeV} \qquad \text{(dipole model)}, \tag{17}$$

$$m_A = 0.85^{+0.13}_{-0.06}\ \text{GeV} \qquad \text{(z expansion with } |a_k| \leq 5\text{)}, \qquad (18)$$

$$m_A = 0.72^{+0.12}_{-0.05}\ \text{GeV} \qquad \text{(z expansion with } |a_k| \leq 10\text{)}. \qquad (19)$$

These values are in good agreement with results from Bhattacharya, Hill, and Paz in [8].

We must note that an issue occurred during this calculation. For $Q^2_{max} \leq 0.2\ \text{GeV}^2$ and bounds of $|a_k| \leq 5$, the chi-squared minimization gave error intervals that extended to negative values. Of course, this is impossible since m_A cannot be negative. Recall, with z expansion, we know $m_A \equiv \sqrt{\frac{2F_A(0)}{F'_A(0)}} = 1.19\sqrt{-\frac{a0}{a1}}$. Furthermore, $a_0 \equiv F_A(0) = -1.269$. Letting $k_{max} = 1$ gives a chi squared function dependent on one variable, that is, a_1. To investigate this issue, we plotted the chi squared function with respect to the variable a_1. The following plot (figure 3) gives insight into the problem.

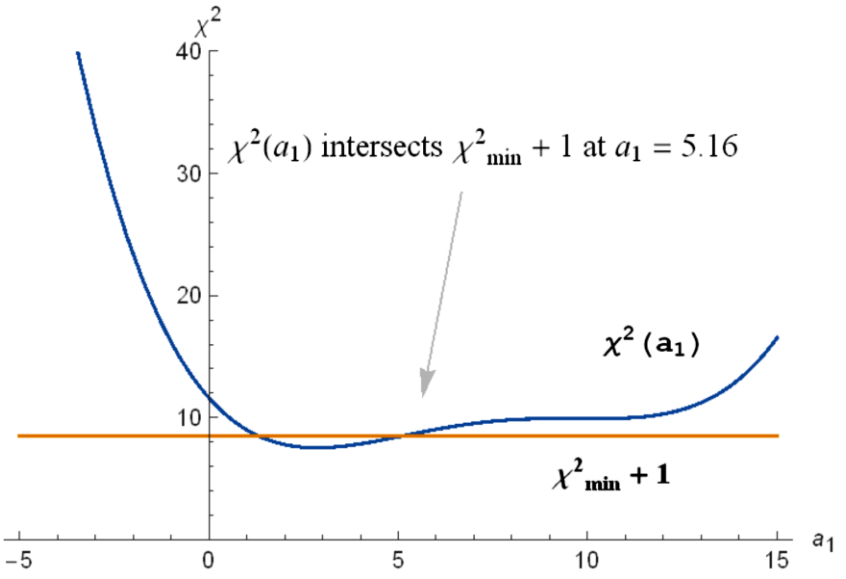

Figure 3: χ^2 as a function of a_1. The error interval is determined by $\Delta\chi^2 = 1$. At the χ^2, $\chi^2_{min}+1$ intersection, $a_1 = 5.16$.

The magnitude of a_1 at $\chi^2 = \chi^2_{min}+1$ is slightly larger than 5. The original constraint was to set $|\mathbf{a_k}| \leq 5$. To solve this dilemma, we unbound the a_1 coefficient when necessary for all further analysis while keeping the bounds on the other a_k. This was applied for the z expansion extraction with $|\mathbf{a_k}| \leq 5$ and $Q^2_{max} \leq 0.2\ \text{GeV}^2$ on both carbon and mineral oil data.

4.2 Mineral oil data

4.2.1 Extracting m_A from mineral oil data excluding contribution of free protons

To form the theoretical prediction for the mineral oil, we use the method described in section 3. This method assumes that all protons are bound in a carbon nucleus. Results for m_A are presented in the same way as in section 4.1. We compare m_A at $Q^2_{max} = 1.0\ \text{GeV}^2$ below

$$m_A^{\text{dipole}} = 1.22^{+0.04}_{-0.05}\ \text{GeV} \qquad \text{(dipole model)}, \qquad (20)$$

$$m_A = 0.77^{+0.10}_{-0.05}\ \text{GeV} \qquad (z \text{ expansion with } |a_k| \leq 5), \tag{21}$$

$$m_A = 0.68^{+0.11}_{-0.07}\ \text{GeV} \qquad (z \text{ expansion with } |a_k| \leq 10). \tag{22}$$

Again, the a_1 coefficient was unbounded when necessary.

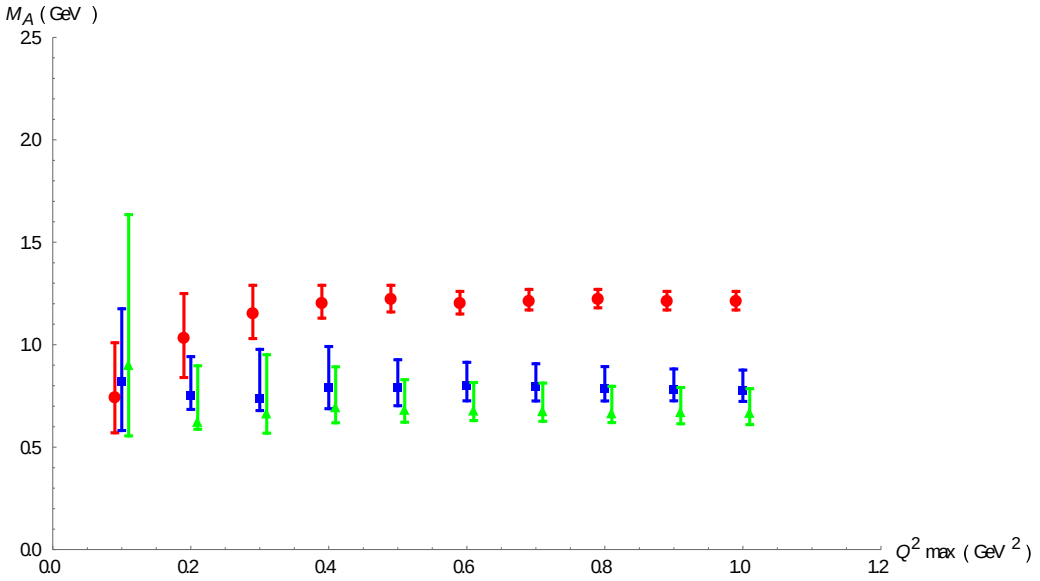

Figure 4: Extracted values of m_A versus Q^2_{max} from mineral oil data with no inclusion of free protons. Dipole model results for m_A^{dipole} are shown by red circles; z expansion results with $|a_k| \leq 5$ are shown by blue squares, and z expansion results with $|a_k| \leq 10$ are shown by green triangles.

4.2.2 Extracting m_A from mineral oil data including contribution of free protons

Recall the composition of the mineral oil, C_nH_{2n+2}, n ~ 20. Letting n = 20, we have $C_{20}H_{42}$. With six protons bound in carbon and one free proton in hydrogen, we have 120 bound protons and 42 free protons in total. Applying these ratios, we obtain the following statistical model,

$$d\sigma_{\text{mineraloil}} = \frac{6.00}{8.06} d\sigma_{\text{carbon}} + \frac{2.06}{8.06} d\sigma_{\text{hydrogen}}. \tag{23}$$

This calculation differs by the formation of the theoretical prediction used in (13). Instead of letting the entire theoretical prediction be calculated using equation (12) for a bound nucleon, we split the prediction into two parts. The carbon component is done in the same manner as before but multiplied by a factor of $\frac{6.00}{8.06}$. For the hydrogen component, we replace equation (12) with the free nucleon double-differential cross section,

$$\frac{d\sigma_{free}}{dE_\mu d\cos\theta_\mu} = \frac{G^2{}_F \left|\vec{P_\mu}\right|}{16\pi^2 m_N} \delta(2pq + q^2)\{2(E_\mu - \left|\vec{P_\mu}\right| \cos\theta_\mu)H_1 + (E_\mu + \left|\vec{P_\mu}\right| \cos\theta_\mu)H_2 - \frac{1}{m_N}[(E_\mu - \left|\vec{P_\mu}\right| \cos\theta_\mu)(E_\nu + E_\mu) - m^2{}_\mu]H_3 + \frac{m^2{}_\mu}{m^2{}_N}(E_\mu - \left|\vec{P_\mu}\right| \cos\theta_\mu)H_4 - \frac{m^2{}_\mu}{m_N} H_5\}, \tag{24}$$

where the H_i are given in [8]. To simplify the calculation, we rewrite the delta function as

$$\delta(2p\cdot q+q^2)=\frac{1}{2m_n-2E_\mu+2\cos\theta\sqrt{E^2{}_\mu-m^2{}_\mu}}\,\delta\left[E_\nu-\frac{m^2{}_\mu-2E_\mu m_n}{2(E_\mu-\cos\theta\sqrt{E^2{}_\mu-m^2{}_\mu}-m_n)}\right]. \tag{25}$$

The flux averaged free nucleon cross section is then

$$\frac{d\sigma_{free,avg}}{dE_\mu d\cos\theta_\mu}=\int dE_\nu f(E_\nu)\frac{d\sigma_{free}}{dE_\mu d\cos\theta_\mu}. \tag{26}$$

The probability density function, $f(E_\nu)$, is calculated from the anti-neutrino flux from Table XI of [1]. By writing the delta function as (25), we can evaluate (26) as follows

$$\frac{d\sigma_{free,avg}}{dE_\mu d\cos\theta_\mu}=\frac{1}{2m_n-2E_\mu+2\cos\theta\sqrt{E^2{}_\mu-m^2{}_\mu}}\cdot f\left(\frac{m^2{}_\mu-2E_\mu m_n}{2\left(E_\mu-\cos\theta\sqrt{E^2{}_\mu-m^2{}_\mu}-m_n\right)}\right)\cdot\frac{d\sigma_{free}}{dE_\mu d\cos\theta_\mu}\left(\frac{m^2{}_\mu-2E_\mu m_n}{2\left(E_\mu-\cos\theta\sqrt{E^2{}_\mu-m^2{}_\mu}-m_n\right)}\right). \tag{27}$$

The experimental data gives double-differential cross section in bins with respect to $\cos\theta_\mu$ and E_μ. We average these bins in the theoretical component by simply evaluating at the center point of the bin. Lastly, we multiply this result by the factor $\frac{2.06}{8.06}$ and sum with the carbon component to obtain the theoretical prediction. Now the chi-squared function is formed in a way that allows hydrogen free proton scattering to contribute.

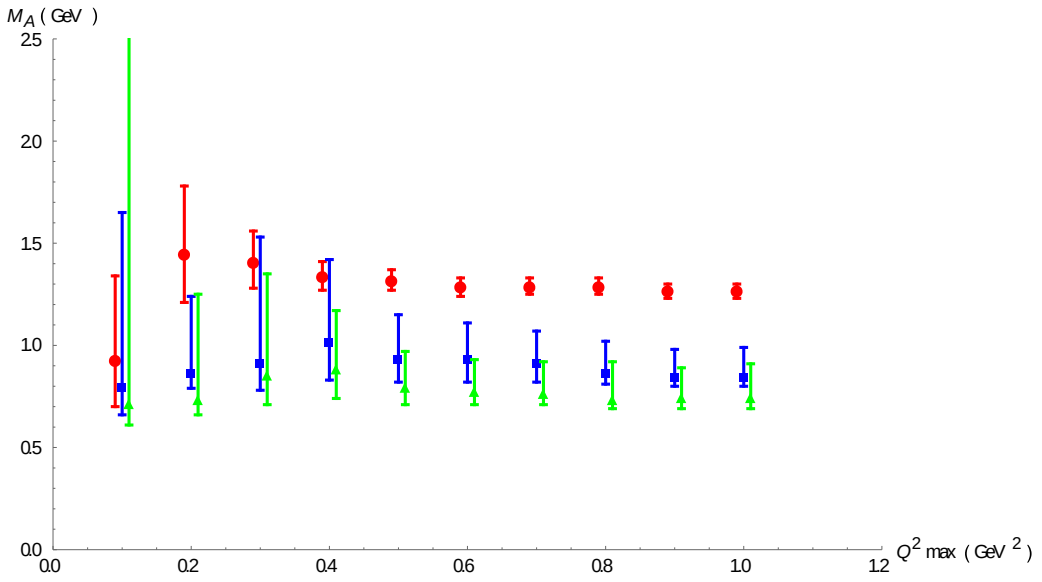

Figure 5: Extracted values of m_A versus Q^2_{max} from mineral oil data with the inclusion of free protons. Dipole model results for m_A^{dipole} are shown by red circles; z expansion results with $|a_k| \leq 5$ are shown by blue squares, and z expansion results with $|a_k| \leq 10$ are shown by green triangles.

Results for m_A are presented in figure 5. Again, we show m_A varying with Q^2_{max} and a comparison at $Q^2_{max} = 1.0$ GeV^2 is made

$$m_A^{dipole} = 1.27^{+0.03}_{-0.04}\ \text{GeV} \qquad \text{(dipole model)}, \tag{28}$$

$$m_A = 0.84^{+0.15}_{-0.04}\ \text{GeV} \qquad \text{(z expansion with } |a_k| \leq 5), \tag{29}$$

$$m_A = 0.75^{+0.16}_{-0.06}\ \text{GeV} \qquad \text{(z expansion with } |a_k| \leq 10\text{)}. \qquad (30)$$

These results are in good agreement with the carbon results in section 4.1.

5 Conclusion

We have described the axial-vector form factor in a model independent manner. This overly constrained form factor could be a source of discrepancy in axial mass values amongst neutrino oscillation experiments. Studies in the past have kept this dipole form factor included in their analysis. Isolating nucleon-level effects before considering nuclear modeling is critical for obtaining a consistent value of m_A. We have shown the effects of hydrogen free proton scattering in the extraction of m_A in the mineral oil data. Figure 6 makes a comparison between values of m_A as extracted by z expansion.

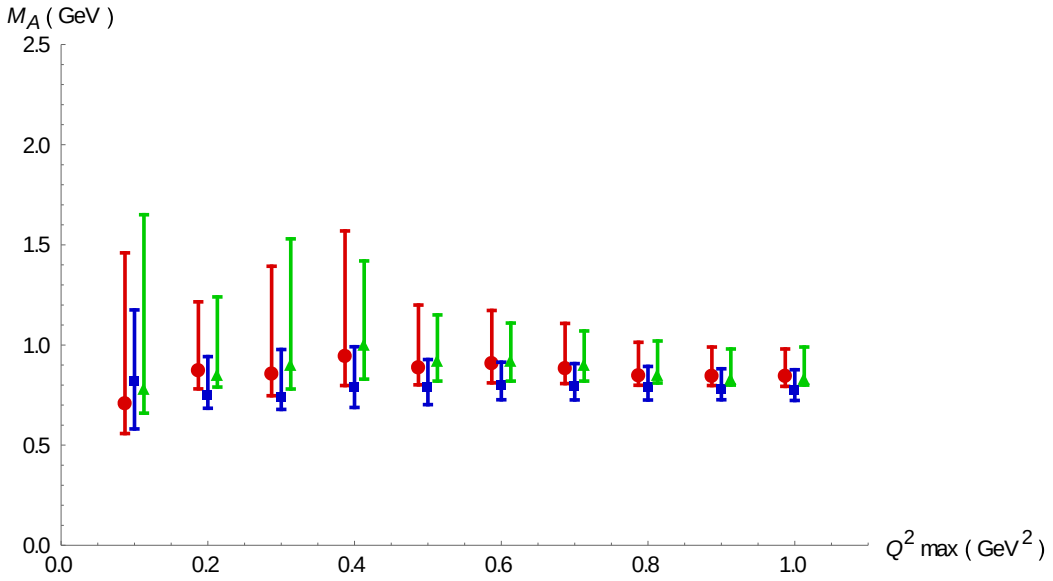

Figure 6: Extracted values of m_A versus Q^2_{max} using z expansion with $|a_k| \leq 5$. Carbon data results for m_A are shown by red circles; mineral oil results without the inclusion of free protons are shown by blue squares, and mineral oil results with the inclusion of free protons are shown by green triangles.

Overall, the results of this paper further indicate that the dipole ansatz is overly constrained producing unreliable values for m_A. Furthermore, we see very good agreement between this anti-neutrino analysis and the neutrino analysis in [8]. The continuation of model independent analysis is necessary for insight into the nature of CCQE interaction. For future work, a similar study can be made on different data sets with a variety of nuclear targets.

Acknowledgements

I would like to thank faculty and staff involved in the Wayne State Physics REU funded by the National Science Foundation through grant PHY-1460853. This summer was a fantastic experience and incredibly beneficial. I had a wonderful time working with the other REU students and participating in the particle theory group with graduate students and faculty. I

would most especially like to thank Dr. Gil Paz for his mentorship on my REU project. I have come a long way in my understanding of modern physics and mathematics. I look forward to continuing work in this area.

References

[1] A. A. Aguilar-Arevalo *et al*. [MiniBooNE Collaboration], Phys. Rev. D **88**, 032001 (2013) [arXiv:1301.7067 [hep-ex]].

[2] V. Bernard, L. Elouadrhiri and U. G. Meissner, J. Phys. G **28**, R1 (2002) [arXiv:hep-ph/0107088].

[3] V. Lyubushkin *et al.* [NOMAD Collaboration], Eur. Phys. J. C **63**, 355 (2009) [arXiv:0812.4543 [hep-ex]].

[4] A. A. Aguilar-Arevalo *et al.* [MiniBooNE Collaboration], Phys. Rev. D **81**, 092005 (2010) [arXiv:1002.2680 [hep-ex]].

[5] R. Gran *et al.* [K2K Collaboration], Phys. Rev. D **74**, 052002 (2006) [arXiv:hep-ex/0603034].

[6] X. Espinal and F. Sanchez, AIP Conf. Proc. **967**, 117 (2007).

[7] M. Dorman [MINOS Collaboration], AIP Conf. Proc. **1189**, 133 (2009).

[8] B. Bhattacharya, R. J. Hill and G. Paz, Phys. Rev. D **84**, 073006 (2011) [arXiv:1108.0423 [hep-ph]].

[9] R. J. Hill and G. Paz, Phys. Rev. D **82**, 113005 (2010) [arXiv:1008.4619 [hep-ph]].

[10] G. Paz, AIP Conf. Proc. 1441, 146 (2012) [arXiv:1109.5708 [hep-ph]].

[11] R. A. Smith and E. J. Moniz, Nucl. Phys. B **43**, 605 (1972) [Erratum-ibid. B 101, 547 (1975)].

[12] J. M. Grange, Ph.D. dissertation, University of Florida, 2013

[13] H. S. Budd, A. Bodek and J. Arrington, arXiv:hep-ex/0308005.

[14] E. J. Moniz, I. Sick, R. R. Whitney, J. R. Ficenec, R. D. Kephart and W. P. Trower, Phys. Rev. Lett. **26**, 445 (1971).